



## ORIGINAL RESEARCH

# A multi-layer framework for energy efficiency assessment of shore-to-ship fast charging systems including onshore batteries

 Siamak Karimi<sup>1</sup>  | Mehdi Zadeh<sup>1</sup>  | Jon Are Suul<sup>2,3</sup>
<sup>1</sup>Department of Marine Technology, Norwegian University of Science and Technology (NTNU), Trondheim, Norway

<sup>2</sup>Department of Engineering Cybernetics, Norwegian University of Science and Technology (NTNU), Trondheim, Norway

<sup>3</sup>SINTEF Energy Research, Trondheim, Norway
**Correspondence**
 Mehdi Zadeh, Department of Marine Technology, Norwegian University of Science and Technology (NTNU), Trondheim, Norway.  
Email: [mehdi.zadeh@ntnu.no](mailto:mehdi.zadeh@ntnu.no)
**Funding information**

Norges Forskningsråd, Grant/Award Number: 493832

**Abstract**

This paper proposes a three-layer framework for energy efficiency evaluation of Shore-to-Ship Charging (S2SC) systems using load-dependent loss models of the components. The considered S2SC system is supplied by the grid but is also supported by On-Shore Batteries (OSB). The presented approach is then used to investigate the impact of the specific design and operational parameters on energy efficiency. Power system architectures for three general S2SC solutions for ac, dc, and inductive charging are defined and compared in terms of energy efficiency. Operational parameters are also considered in the analysis, namely, the grid power ratio, determining the load sharing between the grid and the OSB, as well as the OSB charging profile. A case study is performed with peak charging power of 1 MW, and the most efficient S2SC solutions are identified for both ac- and dc-based onboard power systems. Moreover, it is shown that charging OSB with the highest available power from the grid between the charging breaks would often lead to higher energy efficiency than the maximum utilization of the available charging time. Field data from a real S2SC system is used to verify the estimated energy efficiency by the proposed framework. The analysis of the real case S2SC is then extended to include and verify a projected OSB.

**KEYWORDS**

all-electric ship, energy efficiency, inductive charging, marine electrification, plug-in hybrid electric ship, shore-to-ship charging

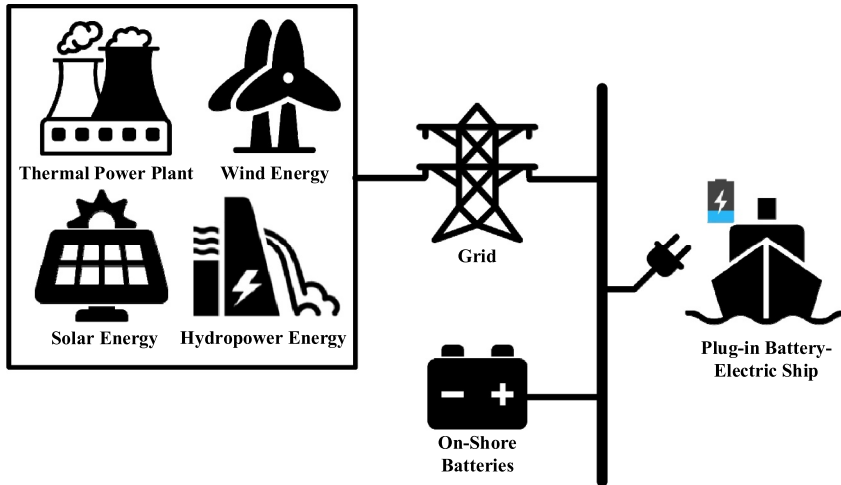
## 1 | INTRODUCTION

Over the last decade, several short-distanced ferries and vessels for coastal transportation have been developed or planned for operating purely on batteries [1, 2]. In fully battery-electric or plug-in-hybrid vessels, the On-Board Batteries (OBB) are recharged from the onshore power grid by a Shore-to-Ship Charging (S2SC) system. As it is illustrated in Figure 1, a S2SC system is considered as a bridge between the onboard loads and Renewable Energy Sources (RES), such as wind, solar, and hydropower [3]. Particularly in Norway, more than 90% of the electric power generation is from hydropower [4]. Thus, the S2SC enables the integration of land-based and offshore RES into maritime transport and paves the way for marine sustainable transformation [5].

Battery-powered marine vessels are nowadays mostly short-distance ships with planned schedules, that is, ferries, which receive charging from shore during the docking period while unloading and loading [6]. For instance, the world's first all-electric car ferry, MF A, operates 34 times per day and receives charging at each 10-min stop between the trips [3]. With such strict limitations of the charging times, it is important to utilise each docking period as much as possible for charging, implying the need for fast charging solutions. However, increasing the charging power can introduce other challenges, such as increased costs and more stress on the local grid. An additional challenge of S2SC for ferries is that they often operate in remote areas with limited capacity of the local power grid, for example, in Norwegian fjords, meaning that the local grid may not be able to provide the high power levels required

This is an open access article under the terms of the Creative Commons Attribution-NonCommercial-NoDerivs License, which permits use and distribution in any medium, provided the original work is properly cited, the use is non-commercial and no modifications or adaptations are made.

© 2022 The Authors. *IET Electrical Systems in Transportation* published by John Wiley & Sons Ltd on behalf of The Institution of Engineering and Technology.



**FIGURE 1** A simple diagram of a S2SC system including OSB

for fast charging [1]. To maintain the possibility of fast charging, the local grids are often supported by stationary energy storage systems, here referred to as on-shore batteries (OSB) [7]. The OSB enables sharing of the charging load and shaves the peak load for the grid by acting as an energy buffer, such that it is charged from the grid when the vessel is away from the dock and is discharged under the high-power charging conditions. However, the OSB introduces additional power losses in the energy flow path, which are associated with the additional power electronics interfaces as well as the onshore battery packs themselves. Hence, energy efficiency is an essential planning factor not only for the ship operators but also for the port authorities. This factor shall be considered in the early design process, and preferably in the contracting stage. In fact, improvement in energy efficiency can result in a lower operational cost, for example, energy cost and equipment maintenance, and on the other hand, can increase the utilization of the available grid power within the critical charging time. The energy loss calculations are one of the necessary inputs for the reliability assessments in the early-phase design stage.

The majority of prior research on marine electrification have focussed on different system topologies of the propulsion systems [8, 9]; the design procedures, including the battery sizing [10]; scheduling [11]; and control strategies for the energy and power management systems [12]. Only a few studies focussed on the challenges of shore-to-ship charging. A review of the charging systems for plug-in battery-powered ships in terms of the power system configuration, current technologies, and control is given in Ref. [3]. The authors in Ref. [6] analysed a harbour-based power system featuring the charging facilities for ships through time-domain simulation. A design approach for the high-power inductive charging for a plug-in hybrid ferry was proposed in Ref. [13] and a full-scale demonstration of this system was presented in Ref. [14]. Also, in Ref. [15] the sensitivity of a high-power wireless charging system for electric ships to the misalignment is studied. Furthermore, a charging strategy for a fully electric ship is assessed in terms of battery sizing and lifetime in Ref. [16], and a techno-economic optimization approach was proposed in Ref. [17].

The efficiency of energy transfer has been widely investigated in land-based microgrids with renewable energy sources and Energy Storage Systems (ESS), [18–23], which can be inspiring for analysis of S2SC systems. However, there are key differences between the shore charging systems, especially for car/passenger ferries, and the land-based systems. The main differentiators are the charging time criticality due to the vessels' schedules; the high-energy demand of the marine batteries, and the grid stress in remote areas where much of the S2SC infrastructure is located [3]. Using stationary batteries in the charging stations to perform ancillary services to the grid, for example, peak-shaving, has been investigated for the EV sector [24]. However, in the S2SC system under study, OSB contributes to supplying the charging loads due to the high load demand. The share of the transferred energy that is delivered directly from the grid (independently from the OSB) can be introduced as an operational variable, namely the Grid Power Ratio (GPR). A preliminary study on the energy transfer efficiency of the S2SC systems was presented in Ref. [25], where only the effect of the GPR was considered as the operating variable.

This paper presents an expanded version of the analysis carried out in Ref. [25], to evaluate the efficiency of the energy transfer from the grid to the OSB in an S2SC system including the OSB. Consequently, the impact of the specific design parameters and operational scenarios on the energy efficiency is investigated. The main contributions of this paper can be listed as follows:

- A three-layer energy efficiency evaluation framework for S2SC systems is proposed, considering load-dependent power loss models for a realistic analysis.
- Based on the proposed framework, different charging solutions such as ac, dc, and inductive charging are evaluated in terms of energy efficiency, and the most energy-efficient S2SC solutions are identified within a range of GPR for various case studies. The case studies consider not only various onshore configurations but also various configurations of the onboard power system, such as ac- and dc-based propulsion.

- The influence of the OSB scheduling on the energy efficiency is also investigated. Suggestions are given for the efficiency improvement under operation.
- For verification, field data from a real S2SC is used and the measured efficiency is compared with the calculated efficiency for the various solutions. The study is also extended to include the integration of OSB.

Hence, the main objective of this paper is to propose an energy efficiency mapping approach that can be utilised in the preliminary design and planning of S2SC systems. At this stage, high-fidelity models may not be needed, while knowing the overall energy efficiency of each charging solution can be crucial [26]. In other words, the proposed framework provides the system designers with an understanding of the main factors influencing energy efficiency as well as estimation of the energy requirement for various charging solutions and technologies. The outcome of this work can be easily employed for component stress and thermal cycling calculations required for reliability/lifetime estimation as well as implementing a power and energy management system to find the optimal operation scenarios.

The analysis is centred around a case study of an S2SC system with 1 MW charging power, where the proposed framework is applied to various charging solutions. The results show that installing onshore batteries deteriorates the energy efficiency of the S2SC solutions differently. For example, for a vessel with an ac-based onboard power system, the dc charging solution is the most energy-efficient solution, although ac and dc charging have the same energy efficiency for the GPR of 1. It is also proved that the inductive charging does not necessarily cause a less efficient charging system than the conductive solutions, even though it adds more power conversion stages, magnetic components and complexity to the system. Considering other advantages of contactless charging, such as reliability, safety, and robustness, these results promote inductive charging as a promising solution. In the end, the available field data on the energy efficiency of S2SC systems is compared with the calculated energy efficiency for the various solutions in this paper. Further, the energy efficiency after installing onshore batteries for examples of real-case S2SC are estimated. To quantify the dependency of the results to the applied parameters, a sensitivity analysis of the calculated energy efficiency in terms of selected parameters is carried out. The proposed framework is also applicable as part of a comprehensive objective function for optimization of S2SC systems by integrating other influencing factors in the design phase, for example, reliability [27], cost, and quay space.

## 2 | SHORE-TO-SHIP CHARGING POWER ARCHITECTURES

The configuration of S2SC infrastructures can vary depending on the available onshore power system. If the grid is not strong enough to supply the high-power charging load, for example,

in rural areas, distributed generation units, such as solar panels and wind turbines, or energy storage systems, namely, batteries and supercapacitors, can be introduced to support the charging load [28]. In this study, the target applications are ferries operating in rural areas with a weak grid, for which the On-shore Batteries (OSB) are considered as the energy buffer to help the grid serve the charging load. The S2S connection is defined as the equipment for connecting the shore bus to the ship, which can be wired through plug systems or wirelessly by inductive power transfer.

A S2SC system consists of four sub-systems: (1) Grid Interface (GI) is the transformer and the rectifier in the dc charging; (2) OSB Energy Storage System (ESS) includes the OSB and its interface converters; (3) Shore-to-Ship (S2S) connection is the interconnection between the shore bus and the to-ship bus; (4) On-Board Charger (OBC) consists of the power components located onboard such as the OBB ESS and the rectifier in ac charging systems. Below, the most relevant S2SC system topologies are described, including ac charging, dc charging, and inductive charging.

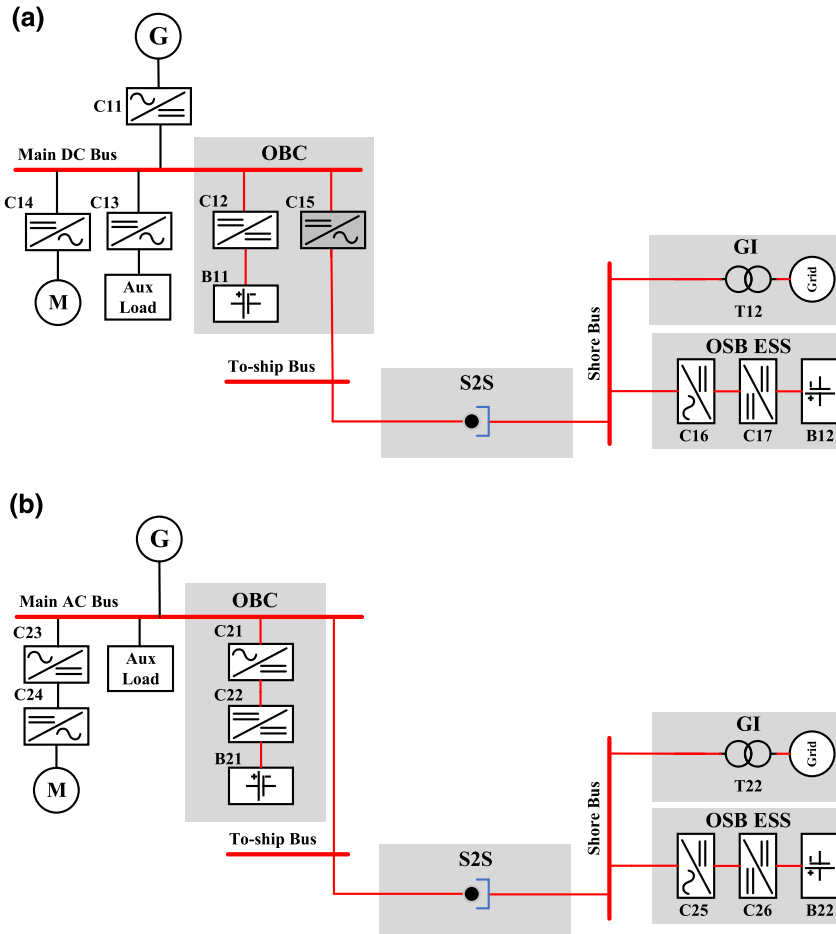
### 2.1 | AC charging systems

In Figure 2a, an ac shore charging power system connecting to a single-bus dc hybrid onboard power system is depicted. The red lines show the charging path from shore to ship. Even though most practical propulsion systems utilise split-bus architectures for ensuring redundancy, only a single bus is drawn for simplicity. The OSB in this topology consists of the onshore batteries B12 and the converters C16 and C17 for interfacing the OSB to the ac shore bus. The power conversion can be a single-stage dc-ac instead of the two-stage with an additional dc-dc converter, but in this case, the battery voltage variation may affect the dc-ac stage. Transformer T12 is a low-frequency transformer stepping down the grid voltage into the shore bus voltage and galvanically isolating the shore bus from the grid. Converter C15, which can be a diode rectifier, an active rectifier, or a power factor correction rectifier, rectifies the received energy from the shore. Among the mentioned alternatives, the diode rectifier is the most efficient solution, although it does not provide power, voltage and power factor control. The bi-directional dc-dc Converter C12 is directly connected to the onboard battery B11 controls transferred power during the charging and discharging process.

In Figure 2b, the grid interface and OSB BESS and S2S connection are the same as those in Figure 2a, but the onboard power system is ac-coupled.

### 2.2 | DC charging systems

There are usually strict volume and weight constraints when designing maritime vessels, especially for pure battery-electric ships. Hence, removing the onboard rectifier (and onboard



**FIGURE 2** The single line diagram of ac S2SC for (a) a dc-based propulsion system and (b) an ac-based propulsion system

low-frequency transformer) to reduce weight and to reduce the number of onboard power conversion stages in the shore-to-ship charging path can be considered as a major step towards increasing the total efficiency and, consequently, the available range of zero-emission battery-based ships. For instance, the “Future of the fjords”, which is an all-electric passenger catamaran made of carbon fibre composite, is using a 1000V dc connection for charging from shore, aiming in reduced weight of the vessel [29]. Figure 3a shows a dc shore charging power system connecting to a single-bus dc hybrid onboard power system. By comparing the power conversion stages in Figure 3a with those in Figure 2a, it can be seen that onboard converter C15 and onshore converter C16 are removed. Further, the grid integration in dc charging includes a rectifier C35, which can be either a diode rectifier as a low-cost and simple solution or an active rectifier, which is more complex but able to control the voltage of the shore-bus. In Figure 3b,a dc shore charging solution for an ac-based onboard power system is shown. The to-ship bus is connected to the input of converter C42, so the charging path is the same as that in Figure 2a. Thus, there is no need for synchronization between the onboard and the onshore power system. Note that if

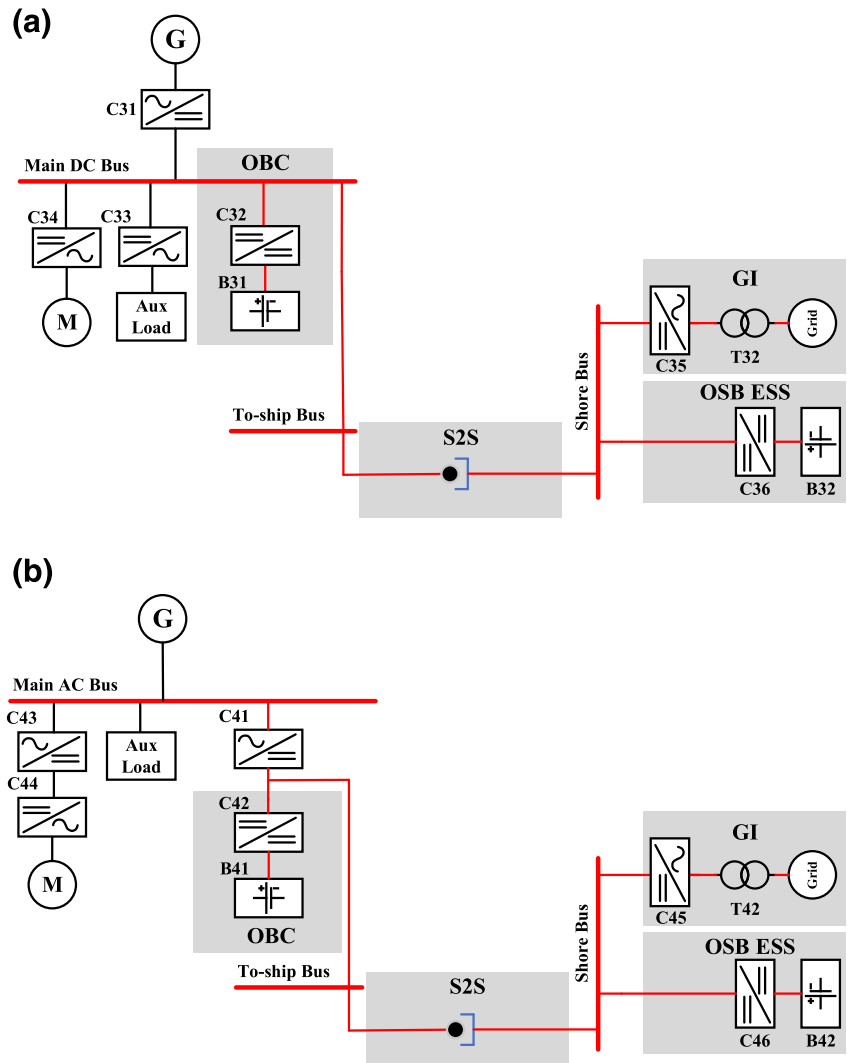
there are any ac loads during the docking, it is better to invert the receiving energy through converter C41, energising the main bus. Although in a dc connection system the conversion stages interfacing the battery to the main bus is reduced and the requirement of synchronization, reactive power control and frequency control are eliminated, the immaturity of the dc protection systems and switchgears for the large and complex systems with multiple busses remain challenging [8].

### 2.3 | Inductive charging systems

In inductive charging, the electric energy is transferred through the magnetic field between the coils rather than conduction through the plug and the receptacle. The most important advantages of wireless charging solution compared to the wired solutions for marine vessels is a more time-efficient operation by eliminating the connection and disconnection procedures, reduced vulnerability to harsh weather and saline water as well as inherent galvanic isolation [30].

In Inductive Power Transfer (IPT), the transmitter and receiver coils act like a transformer with a low mutual

**FIGURE 3** Dc charging for (a) a dc-based propulsion system and (b) an ac-based propulsion system



inductance. The relatively low magnetic coupling results in a high magnetising current, so capacitive compensation networks, P51 and P52 in Figure 4, are used for generating the reactive power consumed by the coils. Converter C56, which is a full-bridge inverter, generates a high frequency (several kHz) square wave voltage. Converter C55 in Figure 4 can be a full-bridge diode rectifier, which converts the high-frequency output of the receiver coil to dc. As it can be seen, transmitter and receiver coils provide galvanic isolation, obviating the need for an onboard low-frequency transformer.

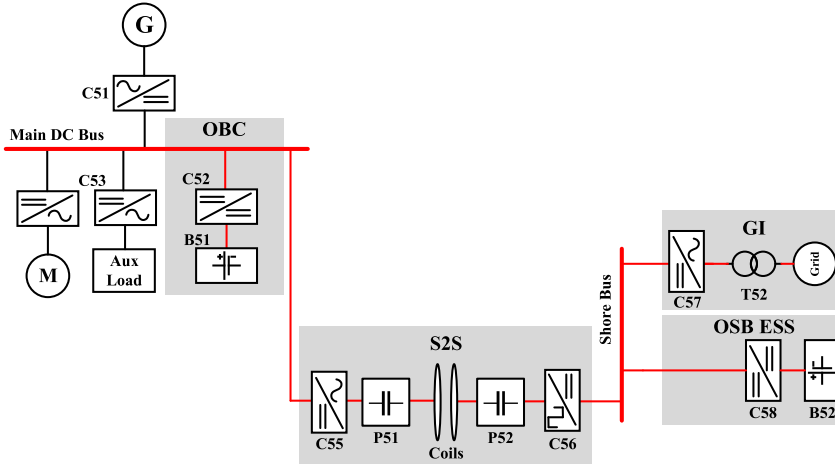
### 3 | SHORE-TO-SHIP CHARGING OPERATION ANALYSIS

The operational analysis and formulation of the charging system is a prerequisite for establishing a realistic energy efficiency model. A short-distance ferry with S2SC at both ends—as a typical battery-driven ship—is considered for the case study. In

a chronological order, the ferry comes to the port for unloading and loading cars and passengers. Subsequently, the shore-to-ship interface, which can be a plug-based connection or a wireless connection, connects and starts transferring power. The charging parameters, usually SoC of the OBB (here called onboard SoC), required charging energy and charging time from the ship side, as well as the available charging power from the shore side, are exchanged between the onboard and onshore control systems. The shore-to-ship data exchange may continue during the charging process until the onboard SoC reaches a certain value or the charging time is over. Then, the shore station reduces the current to zero and disconnects from onboard power system. Notably, in the high-power S2SC systems, the charging profile is usually constant power, and the operating range of the onboard SoC is limited in order to extend the battery lifetime [16].

The power flows in a S2SC system supported by onshore batteries include two terms: the direct pathway from the grid to the OBB and the indirect pathway, which is from the grid to





**FIGURE 4** Inductive charging for a dc-based propulsion system

the OSB and then to the OBB. By neglecting the energy losses, the transferred charging energy to the OBB within one charging break is given by the following expression:

$$E_{OBB-ch} = E_{GI} + E_{OSB-dis} \quad (1)$$

where  $E_{OBB-ch}$  and  $E_{GI}$  and  $E_{OSB-dis}$  are the charging energy stored in OBB as well as drawn energy from the grid and OSB during the OBB charging. Further, due to the practical requirements and simplicity, the battery charging strategy is assumed to be constant power [31]. Thus, the energy flow (1) can be rewritten as following:

$$P_{OBB-ch}t_{ch} = P_{GI}t_{ch} + P_{OSB-dis}t_{ch} \quad (2)$$

where  $P_{OBB-ch}$  and  $P_{GI}$  and  $P_{OSB-dis}$  are the total charging power as well as drawn power from the grid and OSB during the charging time,  $t_{ch}$ . The total charging power is called  $P_{tot}$ , which is equal to  $P_{GI} + P_{OSB-dis}$ . Hence, the GPR is equal to  $\frac{P_{GI}}{P_{tot}}$ , representing the utilization of the OSB for charging the OBB. A simple method for load sharing between the grid and the OSB is that the OSB supply the excessive power if the required charging power is higher than the available grid power. However, scheduling the OSB can play a key role in improving the efficiency, reliability, and operational cost. To do so, the charging power and time for such batteries are determined with respect to the operational conditions. Regarding the charging period for the OSB, similar to Equations (1) and (2), the following equation can be derived.

$$E_{OSB-ch} = P_{OBB-ch}t_{OSB-ch} = E_{G2} = P_{G2}t_{OSB-ch} \quad (3)$$

in which  $E_{OBB-ch}$  and  $P_{OBB-ch}$  are the stored energy and charging power of the OSB within its charging time,  $t_{OSB-ch}$ . Further,  $E_{G2}$  and  $P_{G2}$  are the energy and power drawn from the grid to recharge the OSB. In order to determine the charging characteristics of the OSB between the two charging breaks, the following remarks are considered in this study:

- Due to the unexpected conditions of the ferry operation, the operational characteristics of each trip, such as charging time and trip time, as well as requested charging time, might be variable for 1 day of operation. However, only one cycle starting with the charging break until the ferry comes back to the charging port is considered for energy efficiency evaluation since, due to simplicity, it is assumed that the operational characteristics are constant during 1 day of operation.
- In the real-case energy profiles of the OSB and OBB, due to the practical constraints including the lifetime, the energy discharged from the batteries are not fully recharged in the next charging break [31], resulting in a SoC drop at the end of the day which is compensated during overnight charging. In this work, however, for simplicity, it is assumed that after a charging interval the OSB and OBB are recharged to their initial SoC values.
- The maximum charging power of the OSB is the drawn power from the grid for the OBB charging.

Thus, the following hold true regarding the charging interval of OSB.

$$E_{OSB-dis} = P_{OSB-dis}t_{ch} = E_{OSB-ch} = P_{OSB-ch}t_{OSB-ch} \quad (4)$$

$$t_{OSB-ch} \leq t_{ch} + 2t_{tr} \quad (5)$$

$$P_{G2} \leq P_{G1} \quad (6)$$

In Figure 5, two schemes for calculating the charging power,  $P_{OSB-ch}$  are illustrated. In the first profile, the OSB is charged with the maximum available power, which has been drawn during the OBB charging. As it can be seen in Figure 5a, the OSB is recharged to its initial SoC before the ferry returns to the port. In Figure 5b, the OSB is recharged with the minimum charging power such that the OSB is charged to its initial SoC for the next charging break. Considering the presented operational analysis of the S2SC, in this work, the impact of OSB charging power on the overall energy efficiency is investigated.

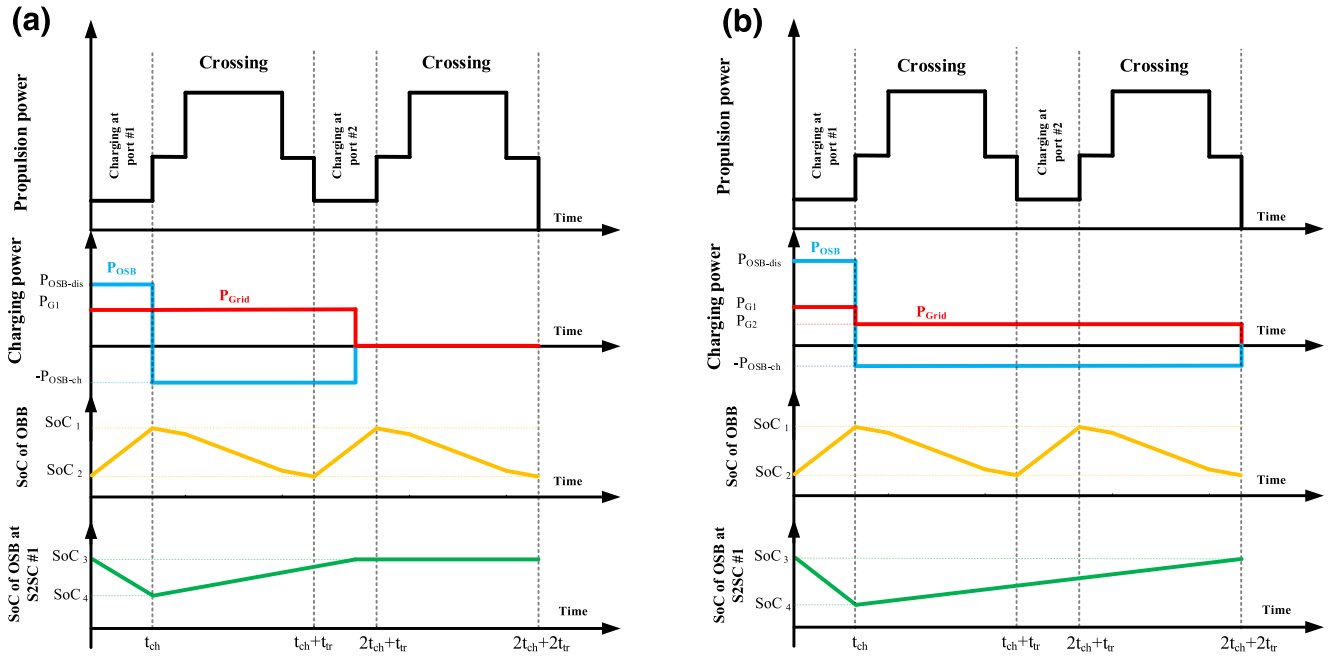


FIGURE 5 The charging profile for a ferry with electric operation within a trip with OSB charging power (a) equal to  $P_{GI}$  and (b) lower than  $P_{GI}$

## 4 | ENERGY EFFICIENCY ASSESSMENT FRAMEWORK

The energy efficiency of the S2SC system is defined as the ratio of the time integral of the charging power to the onboard batteries to the time integral of the drawn power from the power supply over a complete cycle. This energy transfer efficiency from the grid to the OBB depends on the system configuration and components as well as operating and design parameters. As it is depicted in Figure 6, the proposed framework evaluates the energy efficiency of the S2SC system through three layers of hierarchy: A. Component level, B. Sub-system level, and C. System level. In the following, the steps are described individually.

### 4.1 | Component level

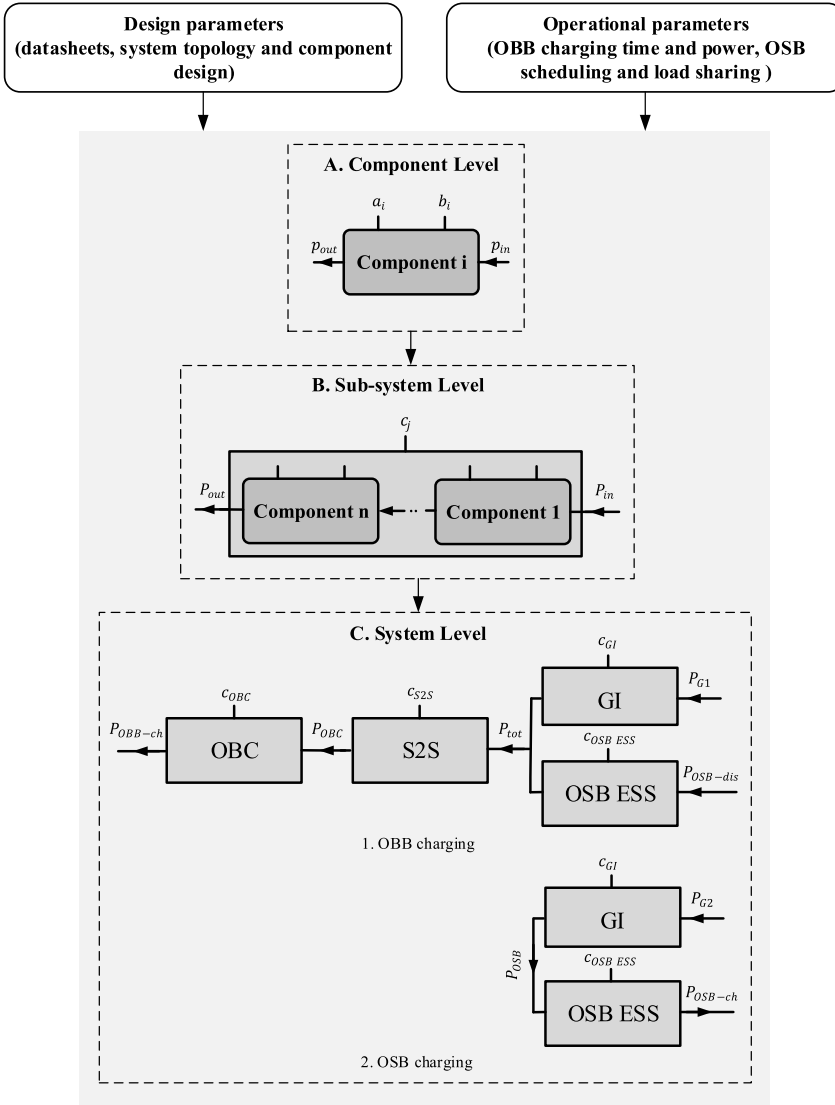
Power converters, as the main components in the charging systems, usually generate the majority of the power loss in such systems [16]. The simplest approach for efficiency modelling of power electronics converters is the analytical averaged power loss models [32]. For each component included in the charging path, a closed form expression for the power loss is introduced in which some approximations and assumptions should be made for simplification. Given that in this work we evaluate the energy efficiency over a several-minute cycle as opposed to the operating point power efficiency, using the time-domain simulations for integrating the instantaneous power loss over the operating period might be time-consuming and tedious. Additionally, rendering the detailed simulations for various configurations and operational scenarios in the design

phase is not preferred. Therefore, the switching events in the power converters are not considered in such models; rather, only the averaged power loss is taken into account, thereby obviating the need for the time-consuming real-time power loss calculations [32]. Since the operation conditions, including the operating power, voltage, current and frequency affect the power loss models, the efficiency models are considered load-dependent rather than constant. Apart from power converters, low-frequency power transformers and filters are modelled with ohmic power loss. Furthermore, the power loss of the Li-ion batteries in OSB is modelled as a function of the SoC and power. The analytical power loss models for all the system components are given in Appendix A. Note that the most common power converter topologies are selected for the S2SC systems analysed here.

The power loss model of the component  $i$  can be written as  $p_{loss,i}(p_{in}, a_i, b_i)$ . The inputs to such generalised power loss models are (1)  $p_{in}$ : input power, represented as, (2)  $a_i$ : the operating conditions, for example, the temperature, terminal voltage, and the switching frequency, and (3)  $b_i$ : design specifications from the datasheets, for example, the turn-on energy dissipation of the IGBT and the passive element values for the dc-dc converter. Hence, the output power,  $p_{out}$ , is calculated as  $p_{in} - p_{loss,i}$ .

### 4.2 | Sub-system level

As it is mentioned in Section 2, an S2SC system consists of four sub-systems: GI, OSB ESS, S2S, and OBC. The configuration of such sub-systems is dependent on both S2SC solution and onboard power system topologies. For example, as it



**FIGURE 6** The three-layer energy efficiency framework applicable for S2SC systems

is shown in Figure 4, the S2S sub-system of the inductive charging is made of power converters and coils. Nevertheless, the S2S sub-system for the dc charging includes only the plug and cables. In general, a sub-system comprises series-connected components. The energy loss of the sub-system  $j$  is obtained as following:

$$E_{\text{loss},j}(t, p, c_j) = \int_0^t \left( \sum_{\forall n \in N_j} p_{\text{loss},n}(p_n, a_n, b_n) \right) dt \quad (7)$$

$$= \int_0^t (P_{\text{out}} - P_{\text{in}}) dt$$

in which  $t$  and  $p$  are the operating time and the input power of the sub-system  $j$ . Moreover,  $N_j$  includes all the components included in the sub-system  $j$ . Furthermore,  $c_j$  indicates the sub-system specification matrix, which contains the operating and design parameters of all the components included in the sub-system  $j$ , and is defined as  $c_j = \bigcup_{\forall n \in N_j} (a_n \cup b_n)$ . Note that  $p_n$

is calculated by the power flow analysis depending on the conversion stage order inside the subsystem and the power flow direction.

### 4.3 | System level

Considering the OBB charging interval depicted in the system-level section of Figure 6, the following energy flow holds true.

$$\begin{aligned} & [E_{GI} - E_{\text{loss},GI}(t_{\text{ch}}, P_{GI}, c_{GI})] \\ & + [E_{\text{OSB-dis}} - E_{\text{loss},\text{OSB ESS}}(t_{\text{ch}}, P_{\text{OSB-dis}}, c_{\text{OSB ESS}})] \\ & - E_{\text{loss},\text{S2S}}(t_{\text{ch}}, P_{\text{tot}}, c_{\text{S2S}}) - E_{\text{loss},\text{OBC}}(t_{\text{ch}}, P_{\text{OBC}}, c_{\text{OBC}}) \\ & = E_{\text{OBB-ch}} \end{aligned} \quad (8)$$

in which  $E_{GI}$ ,  $E_{\text{OSB-dis}}$ , and  $E_{\text{OBB-ch}}$  indicate the energy drawn from the grid, the energy discharged from the OSB, and the energy stored in the OBB. Furthermore, based on the power



flow depicted in Figure 6, during the OSB charging interval, the following energy balance holds true.

$$E_{G2} - E_{\text{loss,GI}}(t_{\text{OSB-ch}}, P_{G2}, c_{GI}) - E_{\text{loss,OSB ESS}}(t_{\text{OSB-ch}}, P_{\text{OSB}}, c_{\text{OSB ESS}}) = E_{\text{OSB-ch}} \quad (9)$$

in which  $E_{G2}$  and  $E_{\text{OSB-ch}}$  indicate the energy drawn from the grid and the energy stored in the OSB due to charging. Given the assumption mentioned in (2), the discharged and charged energy in the OSB is equal for one cycle,  $E_{\text{OSB-ch}} = E_{\text{OSB-dis}}$ . Thus, based on the energy balances in Equations (6) and (7), the energy efficiency from the grid to the onboard batteries,  $\eta_{\text{S2SC}}$ , can be obtained as following:

$$\eta_{\text{S2SC}} = \frac{E_{\text{OBB-ch}}}{E_{G1} + E_{G2}} \quad (10)$$

It is worth mentioning that if the charging energy  $E_{\text{OBB-ch}}$  is lower than the energy used during one trip, the energy efficiency term in Equation (10) must be calculated for the whole cycle of operation. Then, considering  $n$  trips per day and  $E_x^i$  indicates the energy transfer for  $i^{\text{th}}$  trip, the energy efficiency is obtained as following:

$$\eta_{\text{S2SC-d}} = \frac{\sum_{i=1}^n E_{\text{OBB-ch}}^i}{\sum_{i=1}^n E_{G1}^i + \sum_{i=1}^n E_{G2}^i} \quad (11)$$

To better explain the energy efficiency calculation, an example is given in Appendix B.

## 5 | RESULTS AND DISCUSSION

In this section, the energy efficiency evaluation framework presented in Section 4 is applied for various S2SC topologies introduced in Section 2 considering the operational schemes presented in Section 3. In the following, firstly, the case studies and their power component sizing are described. Then, the impact of integration and scheduling of the onshore batteries to the S2SC systems on the energy efficiency of the S2SC system is reported. Further, the energy loss breakdown of the case studies and the available field data are given and discussed. In the end, a sensitivity analysis of the calculated energy efficiency with respect to the critical design parameters is presented.

### 5.1 | Case study description

To perform the analysis for the various configurations, it is required to define the operational and design parameters. The operational parameters including the ship route profile, and OSB, as well as OBB sizing are listed in Table 1. Such

parameters are taken into account for the energy efficiency calculation of all the S2SC solutions under study.

Here, the specifications of each configuration used for the case studies are elaborated in the following.

#### 5.1.1 | AC and DC charging systems

Regarding the ac and dc S2SC systems, as described in Section 2.1 and 2.2, the main design specifications are listed in Table 2 in the following table. Since the nominal charging power is 1 MW, and the minimum of GPR is assumed to be 0.2, all the converters are designed for 1 MW rated power. The dc-dc converters are chosen to be interleaved bidirectional buck/boost converter. Moreover, the topology of the dc-ac converters is two-level voltage source converter. Thus, the IGBT package *FF1500R17IP5P* is chosen [34]. Furthermore, the diode in the rectifier C15 is chosen to be SKKD 701 [35].

#### 5.1.2 | Inductive charging systems

The GI, OSB, and OBC sub-systems of the inductive S2SC system are similar to the case with a dc solution supplying a dc-based ship. However, the S2S sub-system is made up of a full-bridge single-phase inverter, coils accompanied with the compensation network and a single-phase diode rectifier. The IGBTs and diodes for the inverter and rectifier are the same as described previously. The other specifications are listed in Table 3 the following table.

## 5.2 | Impact of installing and scheduling of the onshore batteries

One of the factors affecting the energy efficiency is the GPR, which can be considered as either a design parameter or an operational parameter. To study the impact of such parameter,  $a$  is swept from 0.2 to 1 for the total charging power of

**TABLE 1** Operational Parameters of the case study

Parameter	Value
Nominal S2SC power ( $P_{\text{tot}}$ )	1 MW
Charging time in 1 day ( $t_{\text{ch}}$ )	25 min
Time between two charging breaks ( $t_{\text{tr}}$ )	130 min
OSB capacity and nominal voltage	1000 kWh, 650 V
Li-ion battery internal resistances for charging and discharging @25C [33]	10 m $\Omega$
Number of series and parallel cells (2.3 V and 20Ah each cell)	282, 75
OBB capacity and nominal voltage	650 kWh, 650 V
Number of series and parallel cells (2.3 V and 20Ah each cell)	282, 50

Parameter	Value
Nominal power and voltage ratio of the GI transformers	1 MVA, 11 kV:0.69 kV
Nominal no-load and copper power loss ( $P_{nl}$ , $P_{Cu}$ ) of the GI transformers [36]	2 kW, 10 kW
Grid voltage and frequency	11 kV, 50 Hz
Shore dc and ac bus voltage	980 Vdc, 690 Vac
Main onboard dc and ac bus voltage	980 Vdc, 690 Vac
Voltage and current ratings of the IGBT ( $V_{CE}$ , $I_C$ )	1.7 kV, 1.5 kA
Voltage and current ratings of the diode ( $V_{RSM}$ , $I_{FAV}$ )	1.7 kV, 701 A
Switching frequency of the power converters ( $f_s$ )	2.5 kHz
S2S resistance per phase ( $r_p$ ) [31]	4.75 m $\Omega$

**TABLE 2** Specifications for the ac and dc S2SC systems in the case study

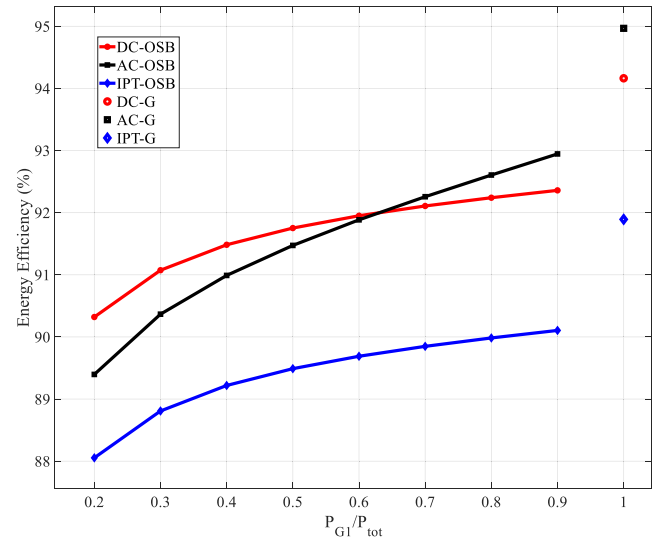
**TABLE 3** Specifications for the inductive S2SC systems in the case study

Parameter	Value
Self-inductances ( $L_t$ , $L_r$ )	400 $\mu$ H
Mutual inductance ( $M_{min}$ , $M_{maxi}$ )	80, 200 $\mu$ H
Coil resistances ( $R_t$ , $R_r$ )	40 m $\Omega$
Resonance frequency ( $f_r$ )	3 kHz

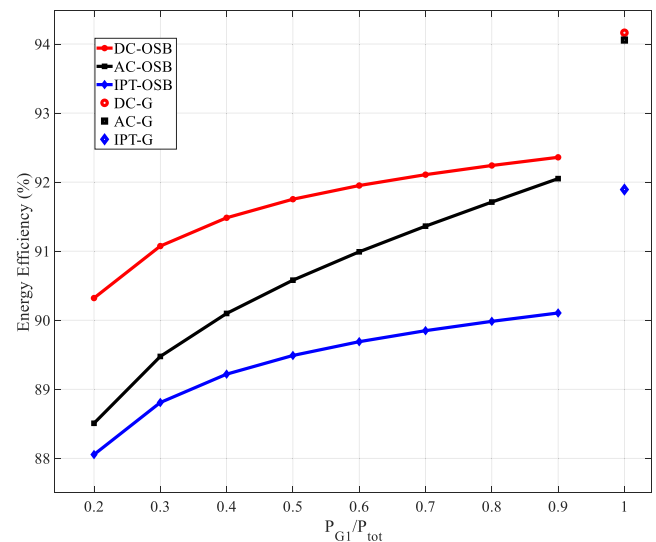
1000kW. Here, the charging and trip times are based on the diagrams shown in Figure 5. Moreover, the selection of the onshore battery charging, as introduced in Section 3, has a significant impact on the energy efficiency. Thus, the calculated energy efficiency for different S2SC topologies in terms of GPR is shown in Figure 7 and Figure 8.

In Figures 7 and 8, the energy efficiency trends are presented for the GPR between 0.2 and 0.9 with the two OSB recharging strategies. Additionally, the efficiency values for the grid-only operation are marked by DC-G, AC-G, and IPT-G. Considering these figures, the following results are deduced. Note that the following remarks may be affected by the applied parameters in this paper, but the purpose of such analysis is mostly comparison between the different charging solutions.

1. By comparing the energy efficiency calculated for grid-only operation and GPR range less than 1 in Figures 7 and 8, it can be concluded that installing onshore batteries reduces the energy efficiency. For example, regarding the dc charging for a dc-based onboard power system, by adding onshore batteries, which contribute to the charging by 10%, the energy efficiency reduces by 1.8%.
2. Furthermore, the lower the ratio of the direct grid power to the total charging power, the lower the energy efficiency of the system. This is because of the energy losses generated in the onshore battery charging and discharging process, including the energy loss dissipated in the power converters and the internal energy loss of batteries.
3. Inductive charging energy efficiency is not far less than that for wired solutions. In fact, zero voltage switching in the inductive charging system causes a reduction of switching



**FIGURE 7** Overall energy efficiency curves for different charging solutions used for dc-based propulsion system



**FIGURE 8** Overall energy efficiency curves for different charging solutions used for ac-based propulsion system

power loss. Although the energy efficiency of dc solution is always higher than that for Inductive solution, wireless charging presents some unparalleled advantages, namely elimination of mechanical issues of plugs and cables and adjustability for harsh weather and sea levels.

4. For a ferry with a main dc bus, the most efficient solution with the applied parameters is dc charging for  $\frac{P_{GI}}{P_{tot}} < 0.6$  as it can be observed in Figure 7. Otherwise, ac charging is the most efficient scenario. In other words, by increasing the share of the grid for charging, the energy efficiency of the ac solution would increase with a higher slope than the other solutions. It is because the voltage source converter C35 in Figure 3 generates more power loss than the diode rectifier C15 in Figure 2 due to IGBT switching power loss. The GI energy loss for dc and IPT are higher than that for ac solution due to its lower number of power conversion stages. In contrast, the OSB energy loss for the ac solution is higher than the others.
5. For a ferry with a main ac bus, the ac charging and dc charging have the same energy efficiency with the grid power ratio of 1 because the power conversion stages are identical. However, as the grid power ratio decreases, the ac charging energy efficiency reduces with a higher slope than dc charging. This is because the energy from the onshore battery is converted into ac at shore bus and converted back to dc to charge the onboard battery in the ac charging. By contrast, in the dc charging system, the onshore battery discharging path to the onboard does not include any dc-ac conversion stages.

To explain the impact of the grid power ratio, the energy loss generated in the onshore direct charging path from the grid to the OBB and the indirect charging path from the grid

to the OSB and then to the OBB are drawn in Figure 9. Note that the configuration of GI and OSB sub-systems for inductive charging is similar to those for dc charging.

It can be concluded that the energy loss dissipated in the direct charging path for the dc charging is more than that for the ac charging due to the ac-dc converter in the GI for dc charging.

Considering Equations (2), (3), and (4), the effect of OSB charging power on the energy efficiency for different values of GPR is investigated and the results are shown in Figure 10.

The impact of the OSB charging power on the calculated energy efficiency can be seen in Figure 10. It can be concluded that for  $\frac{P_{GI}}{P_{G2}} < 2$  and  $\frac{P_{GI}}{P_{tot}} > 0.75$  decreasing the OSB charging power can slightly increase the energy efficiency. This effect is more significant for the dc and IPT S2SC solutions in Figure 10a,b. However, for the other values of  $\frac{P_{GI}}{P_{G2}}$  and  $\frac{P_{GI}}{P_{tot}}$ , the reduced OSB charging power would lead into lower energy efficiency. This phenomenon occurs because the power losses consist of load-dependent and fixed terms, and thus, the calculated energy loss, which is the power loss multiplied by time, can behave as shown. Notably, to calculate the OSB charging power, in addition to the energy efficiency, the electricity price and battery lifetime (charging Li-ion batteries with high power may adversely affect the battery lifetime [37]) must be taken into account.

### 5.3 | Verification and discussion

To fully verify the energy efficiency results, it would be necessary to have access to the energy measurements from full-scale S2SC systems supported by stationary batteries (accounting for OSB) for all the configurations under study.

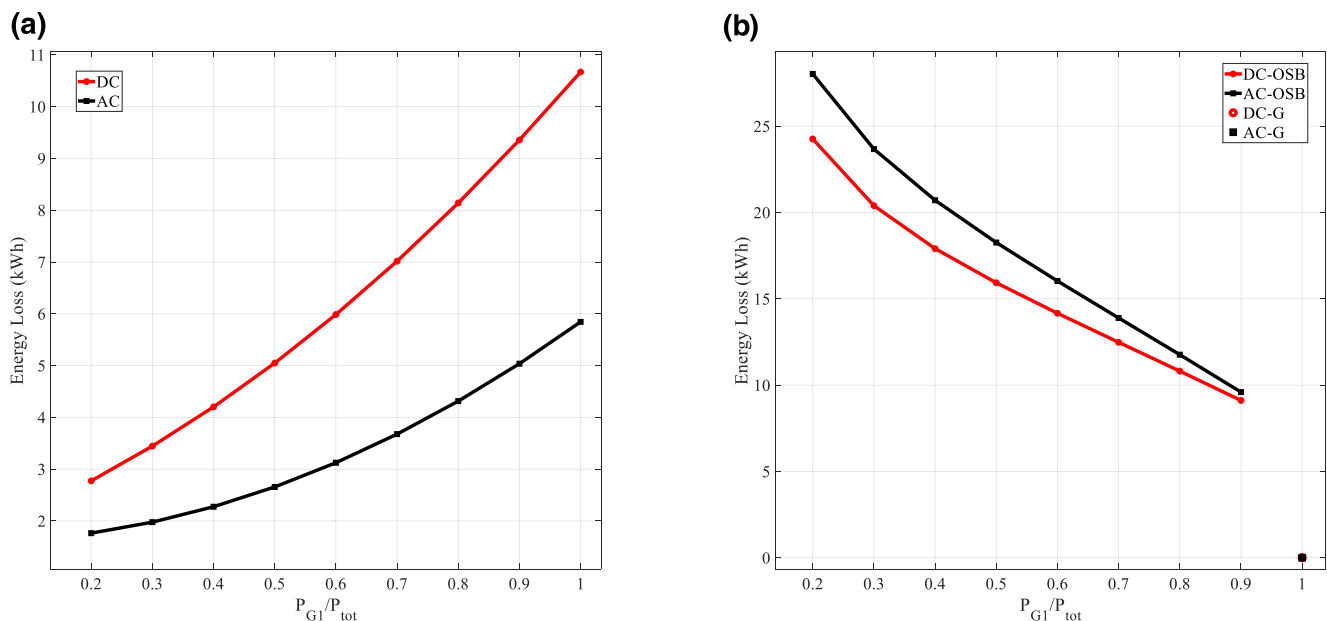
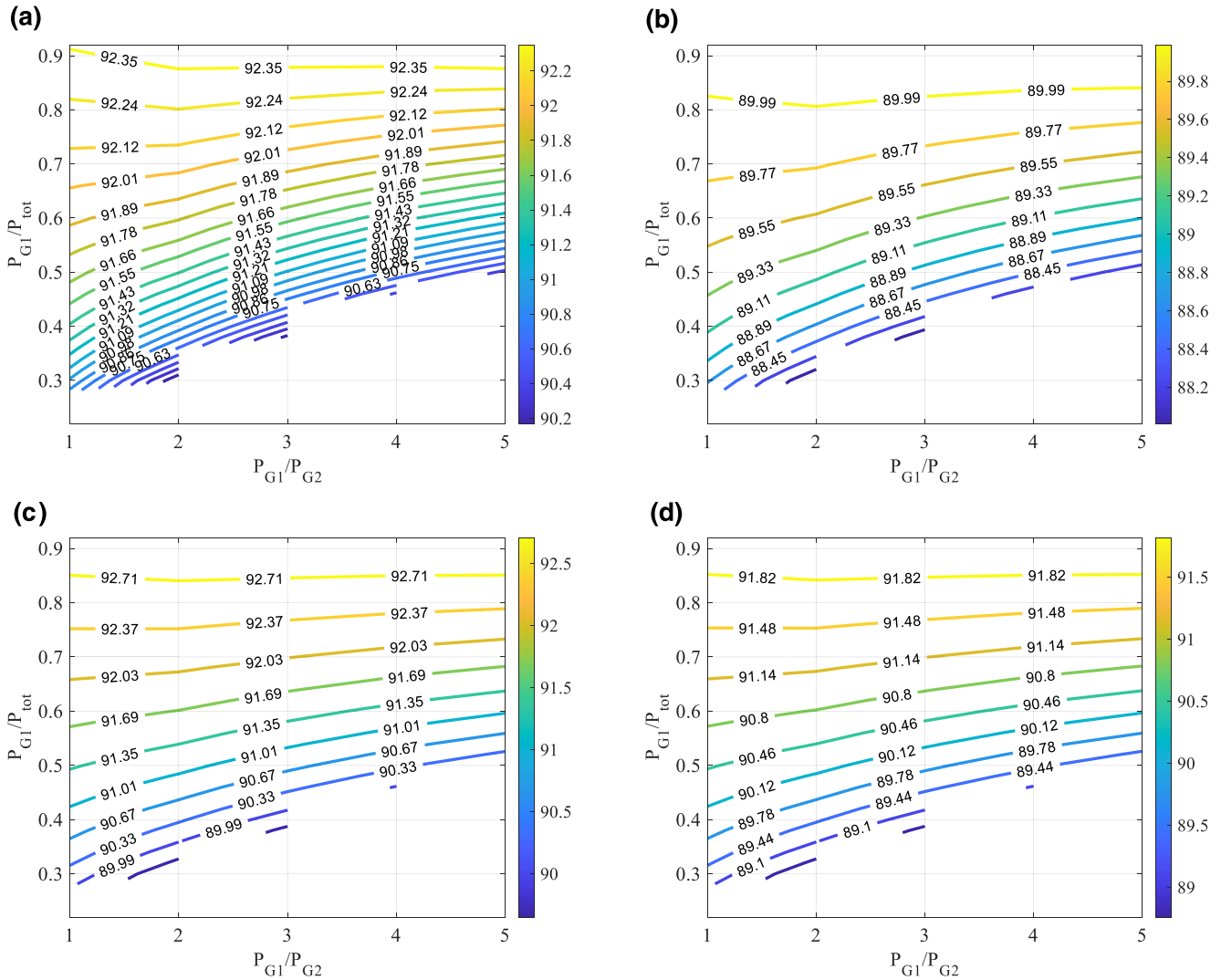


FIGURE 9 Energy loss generated in (a) onshore direct charging path and (b) indirect charging path



**FIGURE 10** The calculated energy efficiency for different GPR and OSB charging power for (a) dc S2SC for dc- and ac-based onboard system, (b) IPT S2SC for dc- and ac-based onboard system, (c) ac S2SC for dc-based onboard system and (d) ac S2SC for ac-based onboard system

However, the power loss models used in this study have been verified by the experimental results in the literature separately. Furthermore, the focus of this study is not the detailed design of S2SC systems. Rather, the intention is to effectively assess the energy efficiency in a preliminary design phase for identifying the influencing factors and give a comparative evaluation of different charging solutions, considering all the relevant design and operating factors. To the best of the authors' knowledge, to this day, only the technical evaluation report of E-ferry Ellen can be a candidate as a publicly available benchmarking reference [31]. In this report, the grid to the OBB energy efficiency for the peak charging power of 4 MW within 25–35 min of charging through dc charging solution is measured as 92%. In addition to the grid to the OBB energy efficiency, the power loss dissipated in the components is reported. However, no onshore battery is employed in this charging system [31]. Further, regarding the 1 MW inductive charging for MS Folgefonn, the efficiency of its S2S sub-

system, dc to dc efficiency, is reported to be approximately 97%. The energy loss breakdown for three solutions studied in this work and the available field data are compared without onshore batteries as depicted in Figure 11a. Moreover, the calculated energy loss breakdown for  $\frac{P_{G1}}{P_{tot}} = 0.5$  and  $\frac{P_{G1}}{P_{G2}} = 1$  are shown in Figure 11b. To make such energy loss breakdowns, the available field data in terms of power transfer efficiencies are translated into the energy loss using the assumed charging parameters in this work. The applied charging parameters are 1 MW charging power within 25 min with OSB charging by  $P_G$ .

Since the connection voltage for the Ellen charging system and the dc solution in the case study are 780 V and 1000 V, the S2S energy loss of those solutions is different. It can be seen that, regarding the IPT in the case study and the field data from Folgefonn, the difference in their S2S energy loss values is 3% while the voltage levels are equal to each other. Considering Figure 11b, installing onshore batteries in

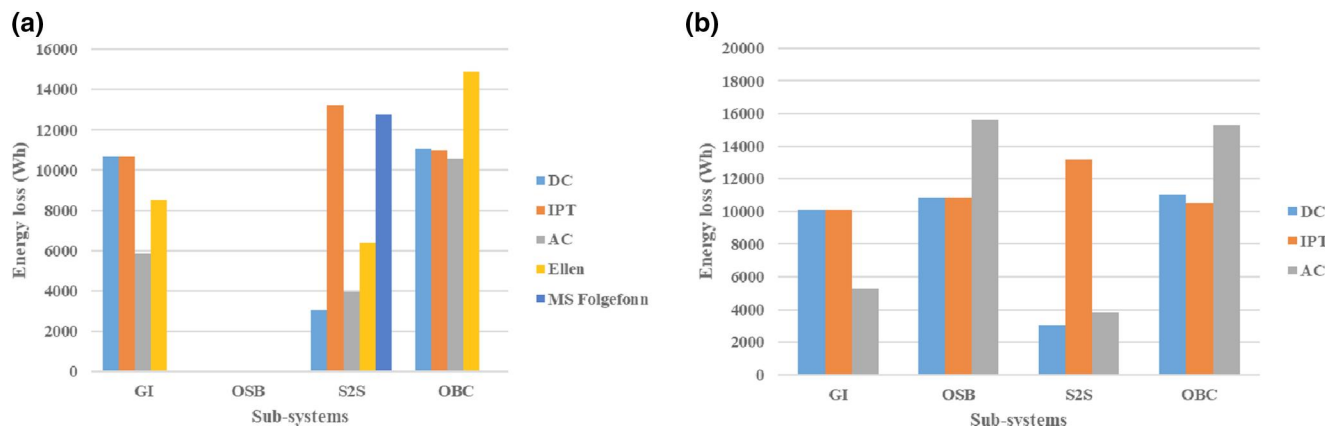


FIGURE 11 Energy loss generated in (a) direct charging path and (b) indirect charging path

the ac solution can lead to high energy loss compared to the other solutions. By comparing the energy loss breakdowns shown in Figure 11, it can be concluded that the energy losses generated in the OBC, S2S, and GI remain approximately constant as the grid power ratio changes. In this regard, the energy efficiency of two real S2SC systems is estimated for grid power ratios of 0.75, 0.5, and 0.25 and depicted in Figure 12.

Considering Figure 12, it can be concluded that by the integration of OSB for the two real-case S2SC systems with inductive and dc charging, by the GPR of 0.5, an energy efficiency of 90% and 88% is expected. Although the energy efficiency can be reduced by adding OSB, the charging capacity is increased, thereby relieving stress on the grid, improving reliability, and extending the ferry operation.

#### 5.4 | Sensitivity analysis

Since the results may be vulnerable to parameter variations and operating conditions, apart from the main three influential factors, a sensitivity analysis is carried out for selected critical parameters. Hence, a sensitivity Indicator (SI) is introduced for each variable for the calculated energy efficiency as following [38].

$$SI = \frac{(\eta_b - \eta_I)/\eta_b}{(X_b - X_I)/X_b} \quad (12)$$

In this expression,  $\eta_b$  and  $\eta_I$  are the base and test values of the calculated energy efficiency, and  $X_b$  and  $X_I$  are the base and test values of the selected parameter. For the inductive charging solution, the resonant network resistances, which is the sum of the resistances of coils and compensating capacitors are considered for the sensitivity. However, since the misalignment between the coils is adjusted by the controller through the change of the switching frequency based on the control scheme described in [14, 15], the power loss of the inductive power transfer resonance network is almost

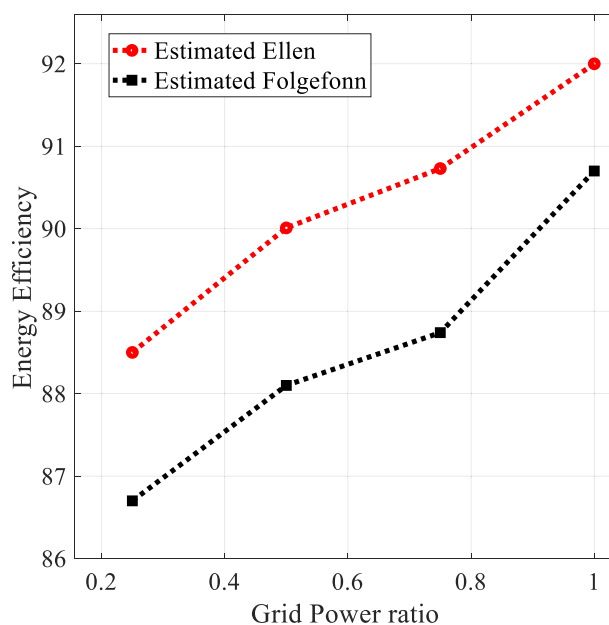


FIGURE 12 The estimated energy efficiency in terms of grid power ratio by installing onshore batteries for the real case S2SC systems

independent of the mutual inductance variations. For the wired solutions, the plug resistance is considered. Moreover, the energy loss generated in the onshore batteries is one of the dominant energy loss terms in the S2SC system. Hence, the sensitivity of the energy efficiency to the internal resistance of batteries, in addition to the plug and coil resistance, is analysed. The results are listed in table 4.

Looking at the calculated SI for the three parameters in the above table, the calculated SIs are less than 0.02. To explain the sensitivity results, for example, if the plug resistance of the dc solution is increased by 100%, the calculated energy efficiency would decrease by 0.74% (from 91.95% to 91.21%). Further, the sensitivity of the energy efficiency with respect to the coil resistance for the wireless topology is approximately two times the sensitivity in terms of the plug resistance for the wired solutions.



Parameter	Parameter change	IPT	dc	ac
Energy efficiency (%)	0%	89.68	91.95	91.88
SI for coil resistance	+100%	-0.0164	-	-
SI for plug resistance	+100%	-	-0.0074	-0.0096
SI for battery internal resistance	+100%	-0.0076	-0.0067	-0.0063

**TABLE 4** Sensitivity analysis results for 1 MW total charging power and grid power ratio of 0.8

## 6 | CONCLUSION

In this paper, the power system architecture and design of the S2SC systems are investigated and evaluated in terms of energy efficiency. For this objective, a three-layer efficiency framework has been proposed based on the component loss models. The presented system architecture includes the components and configurations of various feasible wired and wireless S2SC systems for both dc- and ac-based onboard power systems. In the first layer of the proposed framework, the load-dependent power loss models of the components are derived. Then, the power loss models of components in the sub-systems were integrated together to calculate the energy loss. In the end, considering the operational parameters, namely, the grid power and onshore battery scheduling, the energy efficiency was calculated.

The presented results illustrate how the energy efficiency decreases when the grid power ratio decreases. Further, it is proven that the load sharing between the grid and OSB has a significant impact on which solution is the most energy efficient one for a specific onboard power system. For example, for the dc-based vessel, the ac charging and the dc charging solutions are the most efficient solutions when the grid power ratio is close to 1 and 0, respectively. Moreover, the result shows that wireless charging is a promising solution as it brings just marginally lower efficiency compared to its significant practical advantages over wired solutions.

This framework can be integrated with the other influencing factors, such as reliability, investment and operational costs, quay space, and grid conditions, establishing an early-stage design routine for S2SC systems. Such a design tool can determine which charging solution works best for a specific set of design and operational conditions, namely, the configuration of the onboard power system and available onshore infrastructure. It can also be utilised for the design of S2SC with locally integrated RES, for example, photovoltaic panels, wind turbines, and biomass generators. Another impact of this work is to shape an optimization function for planning the ship charging sequences, within the constraints, as well as the OSB charging and discharging scheduling.

## ACKNOWLEDGEMENT

This work is supported by Norges Forskningsråd, (Grant/Award Number: '493832').

## CONFLICT OF INTEREST

The author declares that there is no conflict of interest that could be perceived as prejudicing the impartiality of the research reported.

## DATA AVAILABILITY STATEMENT

The data that support the findings of this study are available from the corresponding author upon reasonable request.

## ORCID

*Siamak Karimi*  <https://orcid.org/0000-0003-0998-5494>

*Mehdi Zadeh*  <https://orcid.org/0000-0002-9790-537X>

## REFERENCES

- Eide, M.S.: Charting a Course for Green Coastal Shipping. DNV.GL (2016)
- DNV-Maritime.: Alternative fuel insights (AFI). [Online]. <https://afi.dnvgl.com/>. Accessed 10 August 2022
- Karimi, S., Zadeh, M., Suul, J.A.: Shore charging for plug-in battery-powered ships: power system Architecture, infrastructure, and control. *IEEE Electr. Mag.* 8(3), 47–61 (2020). <https://doi.org/10.1109/mele.2020.3005699>
- Tellefsen, T., van Putten, J., Gjerde, O.: Norwegian hydropower: connecting to continental europe. *IEEE Power Energy Mag.* 18(5), 27–35 (2020). <https://doi.org/10.1109/mpe.2020.3001417>
- Fang, S., et al.: Toward future green maritime transportation: an overview of seaport microgrids and all-electric ships. *IEEE Trans. Veh. Technol.* 69(1), 207–219 (2020). <https://doi.org/10.1109/tvt.2019.2950538>
- Kumar, J., et al.: Design and analysis of new harbour grid models to facilitate multiple scenarios of battery charging and onshore supply for modern vessels. *Energies* 12(12), 2354 (2019). <https://doi.org/10.3390/en12122354>
- Sæle, H., Istad, M., Garnås, S.: The Benefit of Batteries in a Flexible Distribution Grid. SINTEF Energy Research AS, Trondheim (2018)
- Jin, Z., et al.: Next-generation shipboard DC power system: introduction smart grid and dc microgrid technologies into maritime electrical networks. *IEEE Electr. Mag.* 4(2), 45–57 (2016). <https://doi.org/10.1109/mele.2016.2544203>
- Valera-García, J.J., Atutxa-Lekue, I.: On the optimal design of hybrid-electric power systems for offshore vessels. *IEEE Trans. Transp. Ele.* 5(1), 324–334 (2019). <https://doi.org/10.1109/tte.2018.2883870>
- Barrera-Cardenas, R., Mo, O., Guidi, G.: Optimal sizing of battery energy storage systems for hybrid marine power systems. In: 2019 IEEE Electric Ship Technologies Symposium (ESTS), Washington (2019)
- Shang, C., Srinivasan, D., Reindl, T.: Economic and environmental generation and voyage scheduling of all-electric ships. *IEEE Trans. Power Syst.* 31(5), 4087–4096 (2016). <https://doi.org/10.1109/tpwrs.2015.2498972>
- Park, D., Zadeh, M.: Modeling and predictive control of shipboard hybrid DC power systems. In: *IEEE Transactions on Transportation Electrification* (2020)
- Guidi, G., Suul, J.A.: Minimization of converter ratings for MW-scale inductive charger operated under widely variable coupling conditions. In: *Proceedings of the IEEE PELS Workshop on Emerging Technologies: Wireless Power, 2015 WoW, Daejeon* (2015)
- Guidi, G., Suul, J.A.: Minimizing converter requirements of inductive power transfer systems with constant voltage load and variable coupling conditions. *IEEE Trans. Ind. Electron.* 63(11), 6835–6844 (2016). <https://doi.org/10.1109/tie.2016.2582459>
- Haque, M.S., Mohammad, M., Choi, S.: Sensitivity analysis and controller design of high power LCC-LCC compensated wireless battery charging



- for electric ship applications. In: 2020 IEEE Applied Power Electronics Conference and Exposition (APEC) New Orleans (2020)
16. Hoedemaker, S.T.C.: Battery Aging in Full Electric Ships. Master's thesis, Delft University of Technology, (2017)
  17. Trieste, S., et al.: Techno-economic optimization of a supercapacitor-based energy storage unit chain: application on the first quick charge plug-in ferry. *Appl. Energy* 153, 3–14 (2015). <https://doi.org/10.1016/j.apenergy.2015.04.054>
  18. Apostolaki-Iosifidou, E., Codani, P., Kempton, W.: Measurement of power loss during electric vehicle charging and discharging. *Energy* 127, 730–742 (2017). <https://doi.org/10.1016/j.energy.2017.03.015>
  19. Schimpe, M., et al.: Energy efficiency evaluation of a stationary lithium-ion battery container storage system via electro-thermal modeling and detailed component analysis. *Appl. Energy* 210, 211–229 (2018). <https://doi.org/10.1016/j.apenergy.2017.10.129>
  20. Bründlinger, R., et al.: 50530 - the new European standard for performance characterisation of PV inverters. In: 24th European Photovoltaic Solar Energy Conference Germany (2009)
  21. Fang, Z., et al.: Optimal design methodology for LLC resonant converter in battery charging applications based on time-weighted average efficiency. *IEEE Trans. Power Electron.* 30(10), 5469–5483 (2014). <https://doi.org/10.1109/tpel.2014.2379278>
  22. Karimi, S., Tahami, F.: A comprehensive time-domain-based optimization of a high-frequency LLC-based Li-ion battery charger. In: 2019 10th International Power Electronics, Drive Systems and Technologies Conference (PEDSTC), Shiraz (2019)
  23. Weniger, J., et al.: Emerging performance issues of photovoltaic battery systems. In: Proceedings of the 32nd European Photovoltaic Solar Energy Conference and Exhibition, Munich (2016)
  24. Rautiainen, A., et al.: Anatomy of electric vehicle fast charging: peak shaving through a battery energy storage—a case study from Oslo. *IET Electrical Systems in Transportation* 11(1), 69–80 (2021). <https://doi.org/10.1049/els2.12005>
  25. Karimi, S., Zadeh, M., Suul, J.A.: Evaluation of energy transfer efficiency for shore-to-ship fast charging systems. In: 2020 IEEE 29th International Symposium on Industrial Electronics (ISIE), Delft (2020)
  26. Sulligoi, G., Vicenzutti, A., Menis, R.: All-electric ship design: from electrical propulsion to integrated electrical and electronic power systems. *IEEE Transactions on Transportation Electrification* 2(4), 507–521 (2016). <https://doi.org/10.1109/tte.2016.2598078>
  27. Karimi, S., Zadeh, M., Suul, J.A.: A Multi-Layer Framework for Reliability Assessment of Shore-To-Ship Fast Charging System Designs. *IEEE Transactions on Transportation Electrification* (2021)
  28. Tsvete, H.A.: Analysis of Charging and Shore Power Infrastructure in Norwegian Ports. *ReCharge* (2017)
  29. Aa, A.: Brodrene Aa and the Fjords pioneering with “Future of the Fjords” – offering zero emission fjord cruise. [Online]. <https://static1.squarespace.com/static/5b18ec3cee1759b32d884907/t/5ca7401a419202c6a737daci/1554464803172/2019+04+Article+Future+of+The+Fjords.pdf>. Accessed 10 12 2019
  30. Guidi, G., et al.: Wireless charging for ships: high-power inductive charging for battery electric and plug-in hybrid vessels. *IEEE Electrification Magazine* 5(3), 22–32 (2017). <https://doi.org/10.1109/mele.2017.2718829>
  31. Kortsari, A., et al.: Prototype and Full-Scale Demonstration of Next-Generation 100% Electrically Powered Ferry for Passengers and Vehicles: Evaluation Report of the E-Ferry (2020)
  32. Al-Naseem, O., Erickson, R.W., Carlin, P.: Prediction of switching loss variations by averaged switch modeling. In: Proc. 15th Annu. IEEE Appl. Power Electron. Conf. Expo, New Orleans (2000)
  33. Li, K., et al.: A practical lithium-ion battery model for state of energy and voltage responses prediction incorporating temperature and ageing effects. *IEEE Trans. Ind. Electron.* 65(8), 6696–6708 (2018). <https://doi.org/10.1109/tie.2017.2779411>
  34. “IGBT modules,” Infineon, [Online]. <https://www.infineon.com/cms/en/product/power/igbt/igbt-modules/>. [Accessed 25 March 2021]
  35. “Rectifier Diode Modules: SKKD 701,” SEMIKRON, (2019)
  36. “HV/LV Distribution Transformers,” Schneider Electric SAS, (2004)
  37. Mussa, A.S., et al.: Fast-charging effects on ageing for energy-optimized automotive LiNi1/3Mn1/3Co1/3O2/graphite prismatic lithium-ion cells. *J. Power Sources* 422(0378-7753), 175–184 (2019). <https://doi.org/10.1016/j.jpowsour.2019.02.095>
  38. Saltelli, A., et al.: Sensitivity Analysis in Practice. A Guide to Assessing Scientific Models. Wiley Hoboken, NJ (2004)
  39. Kolar, J.W., Ertl, H., Zach, F.C.: Influence of the modulation method on the conduction and switching losses of a PWM converter system. *IEEE Trans. Ind. Appl.* 27(6), 1063–1075 (1991). <https://doi.org/10.1109/28.108456>
  40. Wintrich, A., et al.: Application Manual Power Semiconductors. SEMIKRON International GmbH Mendenau, Germany (2015)
  41. Robinson, J., Jovic, D., Joos, G.: Analysis and design of an offshore wind farm using a MV DC grid. *IEEE Trans. Power Deliv.* 25(4), 2164–2173 (2010). <https://doi.org/10.1109/tpwr.2010.2053390>
  42. Vilathgamuwa, D.M., Sampath, J.P.K.: Wireless power transfer (WPT) for electric vehicles (EVs)—present and future trends. In: *Plug in Electric Vehicles in Smart Grids*. Springer, Singapore (2015)
  43. Kjellevoll, A.: Analysis and control of inductive power transfer systems for wireless battery charging in subsea applications. In: Master's Thesis. Norwegian University of Science and Technology, Trondheim (2019)
  44. Tremblay, O., Dessaint, L.-A.: Experimental validation of a battery dynamic model for EV applications. *World Electric Vehicle Journal* 3(1), 1–10 (2009). <https://doi.org/10.3390/wevj3020289>
  45. Nguyen, T.A., et al.: Market evaluation of energy storage systems incorporating technology-specific nonlinear models. *IEEE Trans. Power Syst.* 34(5), 3706–3715 (2019). <https://doi.org/10.1109/tpwrs.2019.2909764>

**How to cite this article:** Karimi, S., Zadeh, M., Suul, J. A.: A multi-layer framework for energy efficiency assessment of shore-to-ship fast charging systems including onshore batteries. *IET Electr. Syst. Transp.* 1–18 (2022). <https://doi.org/10.1049/els2.12052>

## APPENDIX A

The power loss models of the components are listed in Table A1.

TABLE A1 Power loss models of the components


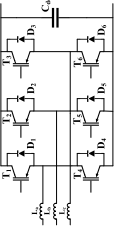

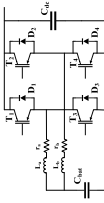

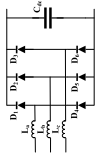
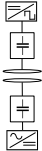
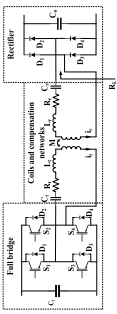


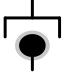
Component	Symbol	Topology	Power loss	Nomenclature	References
Two-level voltage source converter			$P_{\text{Cond loss } T} = \left(\frac{1}{2\pi} + \frac{2D}{8}\right) V_{\text{CH0}} \frac{P_m}{\sqrt{3}V_{ac}} + \left(\frac{1}{8} + \frac{2D}{3\pi}\right) r_{\text{CE}} \left(\frac{P_m}{\sqrt{3}V_{ac}}\right)^2$ $P_{\text{Cond loss } D} = \left(\frac{1}{2\pi} - \frac{2D}{8}\right) V_{\text{FW0}} \frac{P_m}{\sqrt{3}V_{ac}} + \left(\frac{1}{8} - \frac{2D}{3\pi}\right) r_{\text{F}} \left(\frac{P_m}{\sqrt{3}V_{ac}}\right)^2$ $P_{\text{sw loss } T} = \frac{\sqrt{2}f_{\text{sw}}(E_{\text{sw}})}{\pi} \frac{P_m}{\sqrt{3}V_{ac}} \left(\frac{V_{\text{ce}}}{V_{\text{ref}}}\right)^{1.3}$ $P_{\text{sw loss } D} = \frac{\sqrt{2}f_{\text{sw}}(E_{\text{r}})}{\pi} \left(\frac{P_m}{\sqrt{3}V_{ac}}\right)^{0.6} \left(\frac{V_{\text{ce}}}{V_{\text{ref}}}\right)^{0.6}$ $P_{\text{res loss } L} = r_{\text{Lb}} \left(\frac{P_m}{\sqrt{3}V_{ac}}\right)^2$ $P_{\text{loss, ac-dc}} = 6 \left( P_{\text{Cond loss } T} + P_{\text{Cond loss } D} + P_{\text{sw loss } T} + P_{\text{sw loss } D} \right) + P_{\text{res loss } L}$	<p><math>m</math>: Modulation factor</p> <p><math>P_m</math>: Input power.</p> <p><math>V_{\text{ac}}</math>: ac-side voltage</p> <p><math>E_{\text{sw}}</math>: Turning-on and -off energy loss.</p> <p><math>V_{\text{ref}}/I_{\text{ref}}</math>: Voltage and current reference</p> <p><math>V_{\text{CH0}}, r_{\text{CE}}</math>: Equivalent voltage and resistance characteristic of the IGBT.</p> <p><math>f_{\text{sw}}</math>: The switching frequency.</p> <p><math>V_{\text{FW0}}, r_{\text{F}}</math>: Forward voltage and resistance of the diode.</p> <p><math>E_{\text{r}}</math>: Reverse recovery energy loss</p> <p><math>r_{\text{L}}</math>: Resistance of the filter inductor.</p> <p><math>D</math>: Duty cycle</p> <p><math>P_m</math>: Input power.</p> <p><math>V_{\text{bat}}</math>: Battery-side voltage</p> <p><math>E_{\text{sw}}</math>: Turning-on and -off energy loss.</p> <p><math>V_{\text{ref}}/I_{\text{ref}}</math>: Voltage and current reference</p> <p><math>V_{\text{CH0}}, r_{\text{CE}}</math>: Equivalent voltage and resistance characteristic of the IGBT.</p> <p><math>f_{\text{sw}}</math>: The switching frequency.</p> <p><math>V_{\text{FW0}}, r_{\text{F}}</math>: Forward voltage and resistance of the diode.</p> <p><math>E_{\text{r}}</math>: Reverse recovery energy loss</p> <p><math>r_{\text{Lb}}, I_{\text{Lb}}</math>: Resistance and the current of the boost inductor.</p>	[39, 40]
Interleaved bidirectional DC/DC converter			$P_{\text{Cond loss } T} = DV_{\text{CH0}} \frac{P_m}{V_{\text{bat}}} + Dr_{\text{CE}} \left(\frac{P_m}{V_{\text{bat}}}\right)^2$ $P_{\text{Cond loss } D} = (1-D)V_{\text{FW0}} \frac{P_m}{V_{\text{bat}}} + (1-D)r_{\text{F}} \left(\frac{P_m}{V_{\text{bat}}}\right)^2$ $P_{\text{res loss } \text{Lb}} = r_{\text{Lb}} \left(\frac{P_m}{V_{\text{bat}}}\right)^2$ $P_{\text{sw loss } T} = f_{\text{sw}}(E_{\text{on}} + E_{\text{off}}) \frac{D P_m}{I_{\text{ref}} V_{\text{bat}}} \left(\frac{V_{\text{ce}}}{V_{\text{ref}}}\right)^{1.3}$ $P_{\text{sw loss } D} = f_{\text{sw}} E_{\text{rr}} \left(\frac{(1-D) P_m}{I_{\text{ref}} V_{\text{bat}}}\right)^{0.6} \left(\frac{V_{\text{ce}}}{V_{\text{ref}}}\right)^{0.6}$ $P_{\text{loss, dc-dc}} = 4(P_{\text{Cond loss } T} + P_{\text{Cond loss } D} + P_{\text{sw loss } T} + P_{\text{sw loss } D}) + P_{\text{res loss } \text{Lb}}$		[40, 41]

TABLE A1 (Continued)

Component	Symbol	Topology	Power loss	Nomenclature	References
Three-phase diode rectifier			$P_{\text{Cond loss } D} = \frac{2}{3} (V_{\text{FW0}} I_{\text{out}} + r_T I_{\text{out}}^2)$ $P_{\text{res loss } L} = r_{Lb} \left( \frac{P_{\text{in}}}{\sqrt{3} V_{ac}} \right)^2$	<p><math>I_{\text{out}}</math>: The average of the ac-side current.</p> <p><math>V_{\text{FW0}}</math>, <math>r_{\text{FW}}</math>: Forward voltage and resistance of the diode.</p>	[28–40]
Inductive power transformer (IPT)			$P_{\text{loss, diode-rect}} = P_{\text{Cond loss } D} + P_{\text{res loss } L}$ $i_t = \frac{2\sqrt{2}}{\pi} \frac{(V_{ac} R_c + V_{ac} \omega M)}{R_c R_c + (\omega M)^2}, i_r = \frac{2\sqrt{2}}{\pi} \frac{(V_{ac} \omega M - V_{ac} R_c)}{R_c R_c + (\omega M)^2}$ $P_{\text{res } C} = R_c i_r^2 + R_r i_r^2 \text{ (Coils and compensation networks)}$ $P_{\text{cond } D} = \frac{2\sqrt{2}}{2} V_{\text{in}} i_r + r_T i_r^2 \text{ (Rectifier)}$ $P_{\text{sw loss } T} = f_{\text{sw}} (E_{\text{off}}) \frac{k}{V_{\text{ref}}} \left( \frac{V_{ac}}{V_{\text{ref}}} \right)^{1.3} \text{ (ZVS full bridge)}$	<p><math>V_{ac}/V_{\text{bat}}</math>: ac-side in the dc/ac converter and the battery-side voltage in dc/dc converter.</p> <p><math>V_{\text{dc}}/V_{\text{der}}</math>: Transmitter- and receiver-side dc voltage [42, 43]</p> <p><math>E_{\text{off}}</math>: Turning-off energy loss.</p> <p><math>V_{\text{ref}}/I_{\text{ref}}</math>: Voltage and current reference</p> <p><math>V_{\text{CE0}}</math>, <math>r_{\text{CE}}</math>: Equivalent voltage and resistance characteristic of the IGBT.</p> <p><math>f_{\text{sw}}</math>: The switching frequency.</p> <p><math>V_{\text{FW0}}</math>, <math>r_{\text{FW}}</math>: Forward voltage and resistance of the diode.</p>	
Li-ion battery			$P_{\text{Cond loss } T} = V_{\text{CE0}} i_t + r_{\text{CE}} i_t^2 \text{ (Full bridge)}$ $P_{\text{loss, IPT}} = P_{\text{res } C} + 4(P_{\text{sw loss } T} + P_{\text{Cond loss } T}) + P_{\text{cond } D}$ $P_{\text{loss, bat-dis}} = \frac{q}{\omega S} \left[ \left( r + \frac{k}{\text{SOC}} \right) (P_{\text{in}})^2 + kS \left( \frac{1-\text{SOC}}{\text{SOC}} \right) P_{\text{in}} \right] \text{ (discharging)}$ $P_{\text{loss, bat-ch}} = \frac{q}{\omega S} \left[ \left( r + \frac{k}{1-\text{SOC}} \right) (P_{\text{in}})^2 + kS \left( \frac{1-\text{SOC}}{\text{SOC}} \right) P_{\text{in}} \right] \text{ (charging)}$	<p><math>q</math>, <math>v</math>, <math>r</math>: The maximum A hour, nominal voltage, and internal resistance of a battery cell. [44, 45]</p> <p><math>S</math>: The energy capacity.</p> <p><math>k</math>: Coefficient calculated according to the 1-C discharge characteristic V-Ah curve of the battery cell as it is described in [44].</p>	
Power transformer			$P_{\text{loss, trans}} = P_{\text{no load}} + P_{\text{cu}} \left( \frac{P_{\text{in}}}{P_{\text{rated}}} \right)^2$	<p><math>P_{\text{no load}}</math>, <math>P_{\text{cu}}</math>: the nominal no load and copper loss. [25]</p> <p><math>P_{\text{in}}</math>, <math>P_{\text{rated}}</math>: The actual and nominal power.</p>	
Plug and receptable			$P_{\text{loss, plug-dc}} = 2 \left( \frac{P_{\text{in}}}{V_{\text{plug}}} \right)^2 r_{\text{plug-dc}} \text{ (for dc S2S)}$ $P_{\text{loss, plug-ac}} = 3 \left( \frac{P_{\text{in}}}{\sqrt{3} V_{\text{plug}}} \right)^2 r_{\text{plug-ac}} \text{ (for ac S2S)}$	<p><math>r_{\text{plug-dc}}</math>, <math>r_{\text{plug-ac}}</math>: Equivalent resistance of the dc and ac plug. [41]</p> <p><math>V_{\text{dc}}^{\text{plug}}</math>: The voltage of the dc connection.</p> <p><math>V_{\text{ac}}^{\text{plug}}</math>: The RMS value of the line-line voltage of the ac connection.</p>	

<sup>1</sup>In this work, to calculate the efficiency of the IPT, the operation in the resonant frequency without misalignment is considered.

## APPENDIX B

As an example, the energy flow Equations (6) and (7) are explicitly presented in the following for the dc S2SC system connected to a ship with the main dc bus.

Regarding the OBB charging break depicted in Figure B1a, the following holds true.

$$\begin{aligned} & \left[ E_{G1} - \int_0^{t_{ch}} \left( p_{loss,T32}(P_{G1}, a_{T32}, b_{T32}) + p_{loss,C35} \left( P_{G1} - p_{loss,T32}(P_{G1}, a_{T32}, b_{T32}), a_{C35}, b_{C35} \right) \right) dt \right] \\ & + \left[ E_{OSB-dis} - \int_0^{t_{ch}} \left( p_{loss,B32}(P_{OSB-ch}, a_{B32}, b_{B32}) + p_{loss,C36} \left( P_{OSB-ch} - p_{loss,B32}(P_{OSB-ch}, a_{B32}, b_{B32}), a_{C36}, b_{C36} \right) \right) dt \right] \\ & - \int_0^{t_{ch}} \left( p_{loss,S2S}(P_{tot}, a_{S2S}, b_{S2S}) \right) dt - \int_0^{t_{cb}} \left( p_{loss,C32}(P_{OBC}, a_{C32}, b_{C32}) + p_{loss,B31} \left( P_{OBC} - p_{loss,C32}(P_{OBC}, a_{C32}, b_{C32}), a_{B31}, b_{B31} \right) \right) dt \\ & = E_{OBB-b} \end{aligned} \quad (13)$$

Regarding the OSB charging break depicted in Figure B1b, the following holds true.

$$\begin{aligned} & \left[ E_{G2} - \int_0^{t_{OSB-ch}} \left( p_{loss,T32}(P_{G2}, a_{T32}, b_{T32}) + p_{loss,C35} \left( P_{G2} - p_{loss,T32}(P_{G2}, a_{T32}, b_{T32}), a_{C35}, b_{C35} \right) \right) dt \right] \\ & - \int_0^{t_{OSB-ch}} \left( p_{loss,C36}(P_{OSB}, a_{C36}, b_{C36}) + p_{loss,B32} \left( P_{OSB} - p_{loss,C36}(P_{OSB}, a_{C36}, b_{C36}), a_{B32}, b_{B32} \right) \right) dt = E_{OSB-ch} \end{aligned} \quad (14)$$

Then, the energy efficiency is obtained by substituting  $E_{G1}$ ,  $E_{G2}$  and  $E_{OBB-ch}$  in Equation (8).

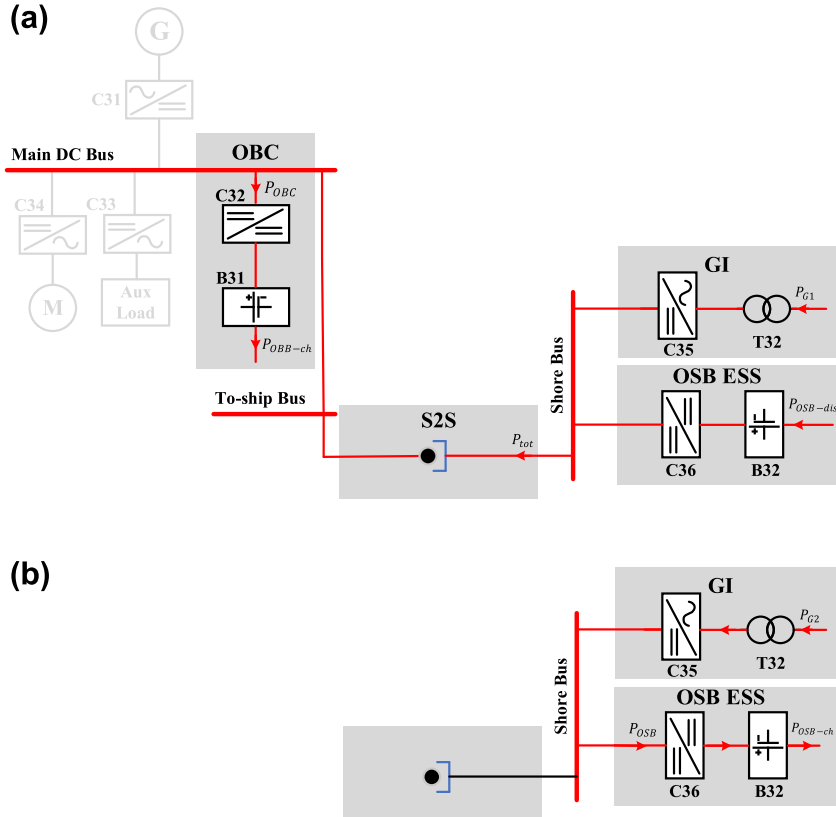


FIGURE B1 An example of power flow while (a) the OBB is charging and (b) the OSB is charging